
Article:
Williams, J., DeLorey, C., Jones, D. et al. (2026) Inchiscope: A Modular Triple-Balloon Soft Robotic Endoscope for Navigating the Small Bowel. IEEE/ASME Transactions on Mechatronics. ISSN: 1083-4435

https://doi.org/10.1109/tmech.2026.3694299

Inchiscope: A Modular Triple-Balloon Soft Robotic Endoscope for Navigating the Small Bowel

Jackson Williams, Charles DeLorey, Dominic Jones, Pietro Valdastri, James Avery, James H. Chandler

***Abstract*—Access to the small bowel remains challenging due to its length, diameter, and curvature, making conventional push endoscopes insufficient for deep exploration. Improved tools that can travel throughout the small bowel without risking mucosal trauma, maintain stable visualisation, and offer fine distal manipulation are needed for diagnosis and targeted treatment of small-bowel diseases. This work presents the Inchiscope, a miniaturised modular self-propelled soft robotic endoscope developed to meet the challenges associated with small bowel access. The presented configuration combines nine independent actuation units to deliver three anchoring balloons and two parallel bellows actuator (PBA) segments for extension/contraction and steering. The modular approach facilitates a minimised diameter (13 mm) while enabling three operation modes including full-body inchworm-inspired locomotion, independent distal segment control for traversing tight bends, and proximal anchoring for stabilised inspection. Characterisation highlights stable anchoring at forces up to 12 N, a PBA elongation ratio of 300 % and controlled omnidirectional bending to 110°. Experiments in rigid and compliant phantoms demonstrate self-propelled locomotion at up to 11.4 mm/s and within tubular environments <25 mm in diameter and with bending radii between 30-45 mm, while the independently actuated distal tip delivered continuous 3D control for observation and positioning in complex geometries.**

***Index Terms*—Soft robotics, enteroscopy, gastrointestinal navigation, medical robotics.**

I. Introduction

THE small bowel is a challenging region for endoscopic intervention due to its considerable length (up to 7 m in adults), narrow lumen (<3 cm), and complex curving geometry [1], [2]. Clinically, reliable access to the small bowel is needed for serious conditions including Crohn's disease, with 6.8 million cases of inflammatory bowel disease (IBD) reported in 2017 [3], and small bowel cancer with over 64,000 cases worldwide predicted for 2020 [4]. Despite surgical intervention, 80% of Crohn's patients require additional surgeries to control disease progression, highlighting a need for minimally invasive tools capable of intervention within the small intestine [5].

This work was supported in part by the Engineering and Physical Sciences Research Council (EPSRC) under grants EP/Y037235/1, EP/V047914/1, and EP/V009818/1; and the National Institute for Health and Care Research (NIHR) Leeds Biomedical Research Centre (BRC) (NIHR203331). Any opinions, findings, and conclusions or recommendations expressed in this article are those of the authors and do not necessarily reflect the views of the EPSRC, or the NIHR. J. Chandler was supported by the Leverhulme Trust and the Royal Academy of Engineering under a RAEng/Leverhulme Trust Research Fellowship (LTRF-2425-21-154).

Jackson Williams, Charles DeLorey, Dominic Jones, James Avery, Pietro Valdastri, and James Chandler are with the STORM Lab, Institute of Autonomous Systems and Sensing (IRASS), School of Electronic and Electrical Engineering, University of Leeds, UK ed20j7w@leeds.ac.uk

Manuscript received xxxx; revised xxxx.

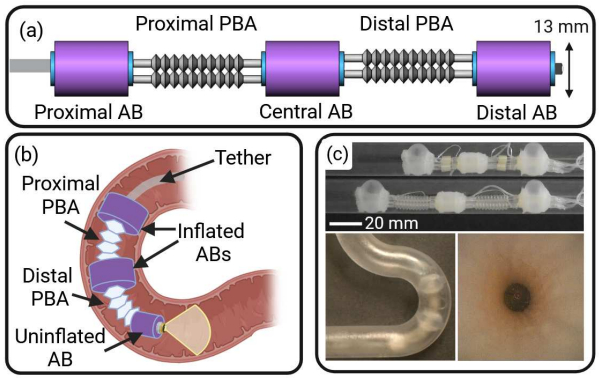

Fig. 1: (a) Inchiscope conceptual design, (b) concept art of Inchiscope navigating a small bowel, (c) snapshots demonstrating navigational capabilities in small bowel phantoms.

Clinical management of these conditions requires tools capable of performing a number of tasks reliably, including: (1) deep navigation into the small bowel; (2) stable anchoring for high-resolution imaging; and (3) precise end-effector manipulation for targeted interventions such as biopsy and drug delivery. Achieving these objectives demands a system that combines effective locomotion with fine distal control, to allow safe and minimally invasive operation throughout the complex small bowel anatomy.

Conventional approaches such as push enteroscopy and balloon-assisted enteroscopy rely on external pushing forces, increasing patient discomfort and risk of mucosal trauma [6]. Double-balloon enteroscopy (DBE), which advances through repeated cycles of balloon anchoring and external force application, is widely used for small bowel access. Of 2,005 device-assisted enteroscopy procedures in the UK over a five-year period, 82% used DBE [7]. Compared with alternative enteroscopy devices, DBE achieves the deepest insertion depth [8], but reliance on external force introduces significant discomfort and typically necessitates sedation [9]. This method also carries a perforation risk of 1.2-1.6% [10]. Entry can be via the upper or lower GI tract; whilst complete exploration from the upper route is possible, it is rarely performed due to increased risk of damage [7]. While DBE provides deep access, the associated trauma risk motivates exploration of self-propelling alternatives. Motorised spiral enteroscopy offers faster, single-operator use, but concerns regarding mucosal injury have led to withdrawal of some systems, reinforcing the need for safer propulsion strategies [11].

As an alternative to traditional endoscope insertion methods, advancement through eversion of material from the distal tip has been proposed [12], [13], [14]. These growing or

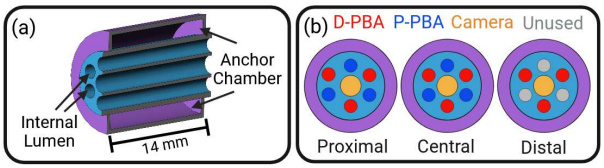

Fig. 2: (a) Cross-section of an AB unit. (b) Routing and connections for the PBAs.

vine robots aim to reduce forces exerted on the environment through lumen-conforming motion. However limitations remain: integrating active precision steering, tool delivery, anchoring, and safe retraction is challenging at small scales [15].

Capsule endoscopy provides tetherless small bowel visualisation, relying on the natural peristalsis to traverse the GI tract. With diameters around 11 mm, these devices enable diagnostics with minimal discomfort, however their passive motion prevents precise positioning or surgical interaction, restricting them to diagnostic use [16]. Therapeutic potential exists via magnetic materials, enabling untethered control, but complex tasks require precise magnetic field manipulation, and force application is limited without anchoring [17].

Active advancement has also been explored through bioinspired locomotion strategies. Earthworm inching uses sequential contraction and relaxation of longitudinal and circumferential muscles to elongate and radially expand body segments, generating forward propulsion [18]. This strategy has been applied to soft robots by creating independent segments for radial expansion and elongation. Several inchworm-inspired endoscopes have been developed for the large intestine [19], [20], [21], but their large diameters ($\sim$20 mm) and slow progression ($\leq$ 3 mm/s in vitro) make them unsuitable for the small bowel. In addition, the common two-balloon, single segment design limits locomotion diversity and hinders independent tip articulation. The Endotics device is an example of a inchworm-inspired colonoscope, which uses a suction anchoring method [21]. Although effective and FDA approved, it has not been miniaturised for small intestine use.

In this work we present the Inchiscope, the first three-balloon, two segment soft robotic inchworm-inspired endoscope designed for deep small bowel navigation. The Inchiscope, Figure 1, achieves a 13 mm diameter miniaturised design while integrating independently actuated proximal and distal sections for precise 3D tip control during locomotion. Unlike conventional enteroscopes relying on external pushing forces, the Inchiscope is fully self-propelling, and its modular configuration enables multiple actuation modes tailored to tasks such as observation, controlled steering to assist in navigation and to aim the camera and tool channel, and anchoring. Enhancements with respect to existing inching designs in miniaturisation, modularisation, and faster locomotion aim to reduce the excessive forces and long procedure times found in DBE [9]. The platform also supports integration of therapeutic tools and sensors for biopsy, drug delivery, and advanced interventions.

II. Methods and Materials

A. Robot System Description

Bioinspired inching locomotion, based on synchronised longitudinal and circumferential expansion/contraction, is a prominent approach in soft robotics, with varied implementations described above and compared in Table I. Notably, the Inchiscope achieves faster locomotion than the prior work and conventional endoscopy. It uses a modular design combining anchoring balloons (ABs) and parallel bellows actuators (PBAs) for adaptable inching locomotion and high dexterity steering. In the proposed design (Figure 1), three identical ABs are separated by two PBA sections (distal and proximal). The ABs are actuated using positive pressure, and expand radially to anchor against lumen walls, while the PBAs can extend or contract under positive and vacuum pressure to push, pull or steer the unanchored sections of the robot.

The AB design was developed to: (1) provide large radial expansion for anchoring across varying lumen diameters, (2) offer internal routing channels for modular connections, pressure lines, electronics and additional clinical tools such as biopsy or drug-delivery tubing, and (3) limit internal deformation under actuation. This is achieved by combining a high stiffness multi-lumen internal core with a lower-stiffness external balloon membrane (Figure 2(a)).

Selection of a PBA for longitudinal propulsion benefits from simple, modular assembly of multiple bellows (Figure 1(a)). The bellows profile enables large bi-directional motion at relatively low material strains, offering lower pressure actuation than other soft pneumatic approaches [22]. Critically, independent bellows motion within each PBA allows omnidirectional bending under differential actuation while still providing large overall contraction/extension when synchronised [23].

By creating a common interface connector, the AB and PBA segments can be reversibly combined and reconfigured to suit specific tasks. For the Inchiscope design, the aim was to deliver independent tip control whilst locomoting; representing a key distinction over existing approaches, and allowing movement and observation dexterity concurrently. To achieve this, the proximal PBA segment is configured to deliver shared actuation pressures to all bellows and thus provides extension and contraction for forward or backward locomotion, while the distal PBA supports independent bellows pressures for extension-contraction or steering control.

B. Manufacturing Process

The ABs of 13 mm diameter and 14 mm length (Figure 2(a)) comprise two parts: an inner multi-lumen section cut from a flexible extruded seven-lumen catheter (Nusil MED-4880 silicone; outer diameter = 6.7 mm, central lumen diameter = 2.3 mm, outer lumen diameters = 1.6 mm, length = 14 mm) and an outer balloon membrane (diameter: 13 mm, length: 10 mm). To manufacture each AB, a hole was pierced into one outer lumen, and a soft tube (ID: 0.02”, OD: 0.037”; McMaster-Carr 51845K66) was inserted and secured with silicone glue (Sil-poxy SmoothOn). A three part 3D printed mould (Form4, Formlabs) was used to cast the balloon membrane in degassed Dragon Skin 10 MEDIUM (SmoothOn) sili-

TABLE I: Comparison of Soft Colonoscopes based on Inching Locomotion

Device	Locomotion	OD [mm]	Elongation [%]	AF [N]	Bend Angle [°]	Speed [mm/s]
Inchiscope (This Work)	**Pneu**	**13**	**300**	**12**	**110**	**8.6 (in-vitro)**
Conventional Colonoscope	EF, CD	13	N/A	N/A	160-180	6.2 (in-vivo)
ROSE [19]	Pneu, CD	26	350	18	180	2.4 (in-vitro), 1.5 (ex-vivo)
SPID [20]	Pneu	18	150	8	130	2.8 (in-vitro)
Endotics [21]	Pneu, CD	20	165	N/A	180	0.6 (in-vivo)

OD: Outer Diameter, AF: Anchoring Force, Pneu: Pneumatic, EF: External Force, CD: Cable-Driven Steering.

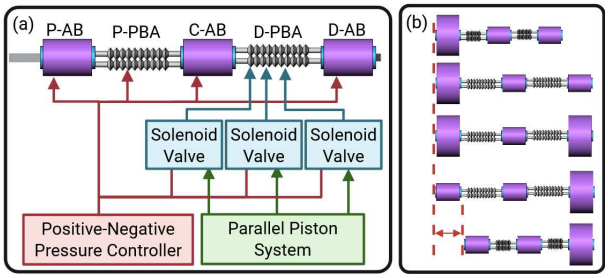

Fig. 3: Inchiscope control overview with (a) control diagram showing the electro-pneumatic controller and volumetric parallel piston system, and (b) Full Extension locomotion cycle.

cone, cured for four hours at room temperature. The membrane was demoulded and bonded to the multi-lumen section with Sil-poxy (SmoothOn), producing a doughnut-shaped balloon with a single inflation inlet. The 2.3 mm central channel routes the camera wiring and pneumatic tubing to distal ABs, while the six 1.6 mm outer channels align and secure the PBA bellows and enable their pneumatic routing, Figure 2(b). The multi-lumen design of the ABs also supports future tool integration: the 2.3 mm central lumen provides sufficient space for the camera wire alongside additional tubing, while three of the six outer lumens in the distal AB remain unused and can serve as dedicated pathways for biopsy tools, drug-delivery lines, or other working-channel instrumentation.

The individual bellows (ID: 2 mm, OD: 4.2 mm, length 29 mm, 10 convolutions) were custom manufactured (Della Medical, LLC) from medical grade TPU (Pellethane 80A). The PBA sections connect to the ABs' outer channels using two connector types: one with an internal airflow channel at the proximal end of each bellows and one sealed to close the pneumatic system. Each PBA comprises three bellows secured at alternating outer AB lumen positions on a 4.48 mm diameter. The two PBA sections, Figure 2(b), are offset to retain independent lumen pathways and actuation.

A 1 mm camera and light source (Ov6948) was routed through the central channel along the robot length and fixed at the distal tip, allowing the distal PBA to position the field of view in three Degrees of Freedom (DoF) inspection during locomotion. The resulting 6.9 g Inchiscope (with an 8.2 g/m tether) has a diameter of 13 mm when ABs are uninflated and is comprised of soft, biocompatible materials for passive compliance, durability and potential medical compatibility.

C. Control Strategy & Implementation

The triple-balloon design of the Inchiscope (Figure 3) enables multiple locomotion strategies to enhance speed and dexterity across diverse endoluminal environments, including straight segments, sharp angulations, and tortuous loops. We consider the primary operational configurations as:

Full Extension Mode: In this configuration, the central AB is idle and both PBAs act in unison as a single extensional segment, achieving an effective doubled stroke length (Figure 3(b)). This allows for rapid movement through straight or less complex segments with improved efficiency.

Front Steering Mode: For locomotion, the cyclic sequence (Figure 3(b)) is again applied, however only the distal and central ABs inflate and deflate to anchor and the distal PBA extends and contracts synchronously to generate forward propulsion. The distal PBA remains free for steering or observation, actuated by the joystick-controlled piston system, providing precise control for navigating sharp bends.

Anchored Observation and Operation Mode: The robot is anchored by the central and proximal ABs, providing a stable platform for independent actuation of the distal PBA bellows. This configuration is suited for high precision tasks such as inspection, biopsy or therapeutic interventions, including polyp removal and targeted drug delivery.

To facilitate this range of locomotion and steering configurations, the Inchiscope requires routing and regulation of vacuum and positive pressures to the ABs and PBA segments (Figure 3(a)). A microcontroller (Arduino MEGA) with PC interface acts as the system controller. Using an I2C DAC (DFR0971, DFROBOT), the microcontroller sets the supply pressures for two electro-pneumatic regulators; (ITV0090-3BL, SMC) for vacuum, and (ITV0010-3BL, SMC) for positive pressure. Each AB connects to an PWM controlled solenoid valve, to set its internal pressure between the positive and vacuum lines.

To selectively route supply pressure to the individual bellows, a 6-port manifold, housing 3-port/2-way 24 V solenoid valves (V114-5LOU, SMC), was used. Digital signals were amplified (MOSFETTI, Adafruit Industries LLC) to 24 V to switch the solenoid valves between vacuum and positive pressure as required. As the proximal PBA operates only in extension-contraction mode for all locomotion configurations in this work, supply lines were connected to a single solenoid valve. However, depending on the locomotion strategy, the distal PBA may require differential pressure across individual bellows (i.e., for steering). Therefore, a separate solenoid valve

connected either to a shared supply for uniform extension-contraction or to independent lines under volumetric control via a parallel piston system detailed below.

Pressure-based control simplifies bellows length modulation, but precision is limited by the non-linear pressure-displacement profile, particularly under vacuum, where the convolutions unfurl/collapse to produce large length changes at near constant pressure. Thus, pressure control was used for extension-contraction PBA tasks, while a volumetrically controlled piston system (Figure 3(a)) was developed to actuate the distal PBA bellows independently for controllable tip steering. Three linear bipolar stepper actuators (Actuonix s20-100-38-b) with 0.01 mm step size were mechanically coupled to pneumatic pistons (CD85N10-100-B, SMC). The operator can switch between modes via a user interface.

D. Individual Bellows and PBA Modelling

Independent control of the distal segment is essential for navigation, observation, and therapeutic tasks in confined anatomy. The distal section is actuated by three parallel bellows arranged symmetrically around the centre of the ABs. For control the commonly employed constant curvature (CC) model is used, approximating the segment as a circular arc with uniform curvature, single-plane bending, constant arc length and no torsion. This simplification enables fast inverse kinematics calculations suitable for real-time control [24].

The CC formulation can be described in three spaces with functions to map between them. (1) The actuator space corresponds to the robot-specific parameters, i.e. the lengths of the individual bellows. (2) The configuration space consists of the arc parameters: average bellows length L, bending angle θ, bending plane ϕ, and curvature κ. Finally, the task space encodes the position and orientation of the tip of the robot.

The independent functions which convert between configuration space and task space for a single constant curvature segment are defined by:

$$\begin{aligned} &x = R\big(1-\cos\theta\big)\,\cos\phi, \quad y = R\big(1-\cos\theta\big)\,\sin\phi, \\ &z = R\,\sin\theta, \end{aligned} \tag{1}$$

where $R = L/\theta$ is the radius of curvature. As $\theta \to 0$, the configuration becomes straight, with $z \to s$ and $x, y \to 0$.

The actuator space describes the lengths of the three parallel bellows arranged around the backbone at radius r and angular positions α_i. The mapping from the configuration space to actuator space is given by:

$$\ell_i \;=\; L \;-\; r\,\theta\,\cos\big(\phi-\alpha_i\big), \qquad i\in\{1,2,3\}. \tag{2}$$

According to this equation, the actuator(s) aligned with the bending direction shorten while the opposite actuator(s) lengthen, providing the desired curvature.

Joystick control was implemented to provide an intuitive interface. The joystick axes, j_x, j_y, were used to encode the bending plane ϕ and angle θ. The arc length L is set using a command-line interface (CLI) to enable more precise positioning in 3D as well as allowing extension and contraction for locomotion. The bending direction is computed as:

$$\phi \;=\; \mathrm{atan2}\big(j_y,\, j_x\big), \tag{3}$$

and the joystick magnitude is:

$$m \;=\; \sqrt{j_x^2 + j_y^2}, \qquad 0 \le m \le 1. \tag{4}$$

This magnitude is mapped linearly to the bending angle:

$$\theta \;=\; m\,\theta_{\max}, \tag{5}$$

where θ_{max} is the maximum allowable bend angle, set to 90° in this work, chosen through preliminary testing. Given the desired arc length L selected via the CLI, the actuator lengths are then calculated using Eq. (2).

This control method provides an intuitive mapping between user input and robot configuration, enabling proportional and continuous adjustments for precise tip positioning during navigation and observation. The simplicity of the CC model ensures low computational cost and predictable motion, while the joystick interface offers user-friendly teleoperation. Additionally, the entire control pipeline is implemented digitally, providing the foundation for automation.

III. Experimental Characterisation

A. Anchoring Balloons

To evaluate the radial expansion characteristics and manufacturing repeatability, each AB was inflated from 0 to 50 kPa in 2 kPa increments while being imaged (acA2040-120ac, Basler) in the radial plane. At each pressure step, the AB was allowed to stabilise for 30 s before an image was captured and processed (ImageJ) to extract the maximum diameter. Each of the three ABs was tested over five repeats, with the median response and range shown in Figure 4(a-I).

The diameter of the ABs was 12.8±0.4 mm (0 kPa) to 41.2 ±1.3 mm (50 kPa), covering the clinically relevant range for a distended small bowel [2]. From 0-20 kPa minimal expansion occurs. However, due to the hyperelastic properties of the AB membrane, a rapid expansion occurs from 20-40 kPa accounting for ∼80% of the total diameter increase. For pressures $>$ 40 kPa a steady, moderate increase in diameter is observed. Variability between trials is low, with overall standard deviation $<$ 2 mm. However, larger variability of between 2 and 7 mm occurs during the rapid expansion region. Between ABs, a similar response is noted, although a small offset in the critical pressure before rapid inflation is evident along with the maximum attained diameter at 50 kPa. After 300 cycles of inflation between 0 and 40 kPa, AB 3 shows some permanent stretching and an earlier period of rapid increase (from 18 kPa), however the overall shape and size of the inflation curve remains similar. During standard operation ($<$ 35 kPa) there was no damage to the ABs. However, bond failure between the inner and outer sections of the AB occurred at high pressures ($>$ 40 kPa) but was easily repaired and prevented using additional silicone glue during the manufacturing step.

To evaluate the anchoring performance of the ABs, the wall contact force and the force during axial loading was measured for different inflation pressures within a 32 mm diameter compliant tube (material: low-density polythene). The AB was first inflated to a target pressure of either 30, 35 or 40 kPa, corresponding to unconstrained diameters of 32, 34 and 38 mm

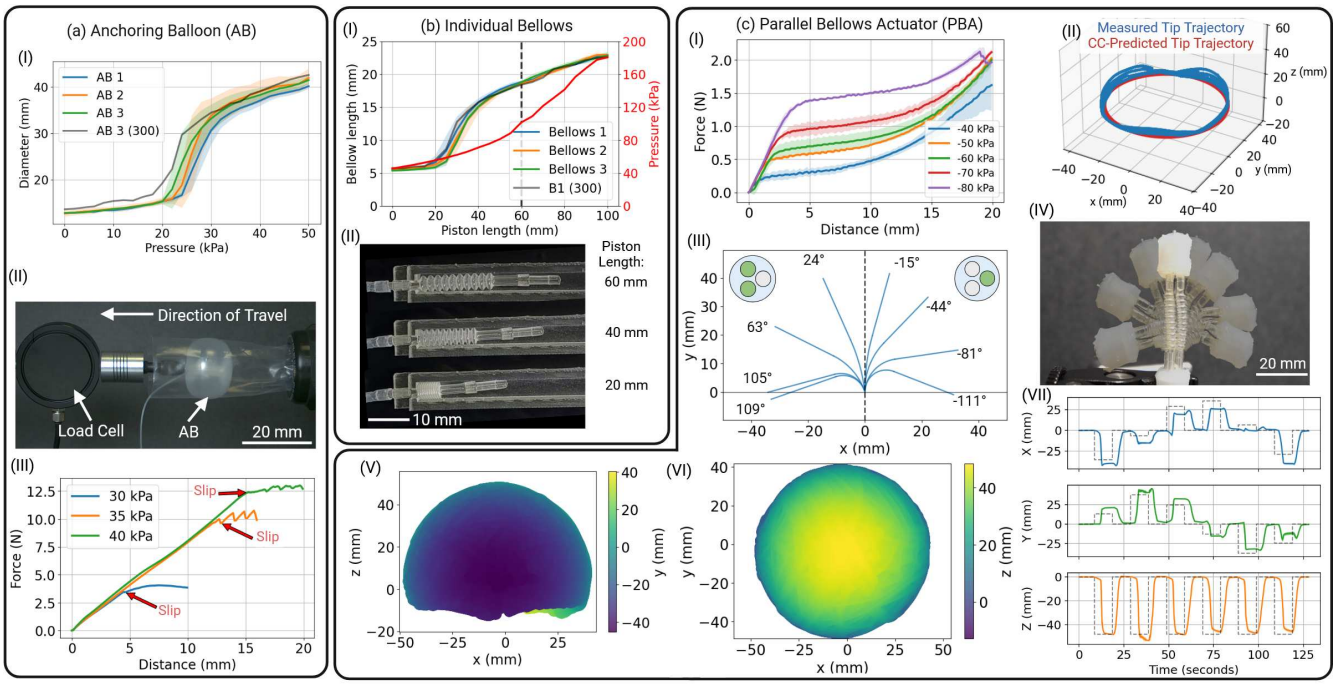

Fig. 4: (a-I) AB inflation characterisation results, including the results after 300 cycles. (a-II) Setup for anchoring characterisation and (a-III) corresponding results. (b-I) Individual bellows extension results, including the results after 300 cycles, and (b-II) setup. (c-I) PBA force characterisation, (c-II) CC-model validation test results, (c-III) PBA bending results, with (c-IV) corresponding overlaid Inchiscope positions. Inchiscope workspace in the (c-V) x-z plane and the (c-VI) x-y plane. (c-VII) Time-series graph showing the dynamic response of the end-effector across 5 repeats, with the targets as dotted lines.

and wall contact forces of 0.4±0.1 N, 0.6±0.1 N, 1.2±0.1 N (measured using a Mouser Electronics MF01-N-221-A04 film force sensor) respectively, with three repeats at each pressure. The AB was pulled using a linear stage (NRT150, Thorlabs) at 4 mm/s while the axial force recorded using an inline load cell (DBCR Compact S-Beam, Applied Measurements, UK), shown in Figure 4(a-II). The slipping point was determined by identifying the first drop in force, indicating the AB moving relative to the tube.

At 30 kPa, the AB resisted a force of 3.8±0.1 N before slipping (4(a-III)). For higher pressures of 35 and 40 kPa, which inflate the AB to diameters larger than the tube, 9.9±0.2 N and 12.4±0.2 N were required to cause the AB to slip, respectively. The results show that higher pressure improves the anchoring strength, providing a secure grip for inching.

B. Independent Bellows Characterisation

Individual bellows were first characterised by comparing the actuator (piston) position with the length of the active part of the bellows, i.e. the convolutions but not the connection ports (Figure 4(b-I)). The internal pressure of the bellows was also recorded for reference using an independent pressure sensor (MPRLS Breakout, Adafruit). The bellows were normalised to atmospheric pressure (∼100 kPa) with the piston at 60 mm. This position was empirically determined to give a suitable bidirectional displacement range to generate the required positive and vacuum pressure for extension-contraction. A quasi-static test was performed by positioning the actuator at 60 mm, then first decreasing to the maximum negative position (0 mm) in 5 mm steps, with an image recorded at each step after a 10 s settling period. This process was then repeated from 60 mm up to the highest positive pressure position (100 mm). Each of the bellows used in the distal PBA were tested over three repeats, as shown in Figure 4(b-II).

The mean±SD length of the active part of the bellows at ambient pressure (actuator position: 60 mm) was 18.7±0.1 mm. Across the range tested, the mean±SD active length varied between 5.5±0.1 mm (actuator position: 0 mm) and 22.9±0.1 mm (actuator position: 100 mm), with the 70% of the 17.4 mm length change (12.5 mm) occurring between actuator positions 20 mm and 60 mm, and pressures 101.6 and 55.4 kPa respectively. Accelerated cycling testing was conducted (300 repeats), however, there was no notable change in performance of the bellows and at no point during usage did any failures occur. It was observed that for actuator positions greater than 60 mm (>100 kPa), the positive pressure caused the linear actuator to occasionally skip steps resulting in a misalignment and incorrect position over a long period of operation. Thus the operational region of the bellows under piston control was set to negative only (actuator positions 0 mm to 60 mm) relating to a extensional ratio for the active part of the bellows of ∼350%; a relatively small decrease compared to the bellows extension over piston position 0 mm to 100 mm (416%). A cubic function was fit ($R^2 = 0.99$) to the data to model the operational region of the bellows piston-length relationship for use under CC-based joystick control.

C. Parallel Bellows Actuators

The distal parallel bellows actuator (PBA) was assembled by mounting three pneumatic bellows in a symmetric arrangement

around the centre of the robot, with ABs attached at both ends. This configuration allows axial contraction for locomotion or omnidirectional bending for tip steering via coordinated actuation of the individual bellows. To simplify these modes of control, each bellows can be driven either under pressure control via positive and negative solenoid valves or volumetric control using the parallel piston system.

For coupled axial contraction, a force test was conducted to quantify the Inchiscope's ability to generate sufficient force for locomotion through the small intestine. The axial force output of the distal PBA was evaluated by fixing one side of the actuator and pulling the opposing end using a motorised linear rail (NRT150, Thorlabs) at 4 mm/s. The axial force was recorded using an inline load cell at 300 ms intervals. Testing was conducted at fixed pressures set by the pressure regulator: -80 kPa, -70 kPa, -60 kPa, -50 kPa, and -40 kPa, with each test repeated three times. The bellows were pulled up to 20 mm in total reaching maximum forces of approximately 2 N. As shown in Figure 4(c-I), the general shape was similar for all pressure levels, with the contraction force increasing rapidly, followed by a plateau and then increasing again gradually. Higher negative pressures resulted in a larger forces.

To evaluate the bending range of the distal PBA, it was configured with one bellows aligned with a bending plane resulting in the plane aligning directly between the other two bellows, allowing identification of range and variation in bending based on the number of actuators. Bending tests were completed by contracting the individual or pair of bellows aligned with the bend direction, with the associated piston(s) moving in 10 mm steps from 60 mm to 20 mm. This was repeated three times. Figure 4(c-III) shows the resultant bidirectional bending of the PBA. The maximum bend angle for the two bellows direction and single bellows direction were similar, 115.3±3.7° vs 111.1±2.6° respectively.

An additional workspace analysis was performed to evaluate the range of motion and reachable positions of the distal segment (PBA with AB), which directly impacts navigation and tool/camera orientation ability within confined anatomical spaces. The full workspace of the distal PBA was determined using a 3D optical tracking system (OptiTrack, Prime 13, NaturalPoint, Inc., U.S.A.) The volumetric parallel piston system was controlled to move the distal PBA randomly within its operational range (piston positions 0 mm to 60 mm) for one hour, generating a comprehensive dataset of reachable positions. As shown in Figure 4(c-V, c-VI), the workspace approximately defines a hollow spherical shape centred at the proximal end of the active region of the PBA with an outer radius of ∼42.6 mm. The lower portion of the sphere saturates (below ∼12 mm) due to the maximum bend angle of the PBA.

To assess the CC-based control, the distal PBA was instructed to trace concentric circles within the reachable workspace. Target points were defined in the configuration space with parameters (L, θ, ϕ) and then mapped to the desired bellows lengths. The inverse of the piston length to bellows length cubic function was used to obtain the required piston positions to reach the desired bellows lengths. For the desired trajectories, the tip of the AB was tracked over five rotations. Figure 4(c-II) shows distal segment trajectories with

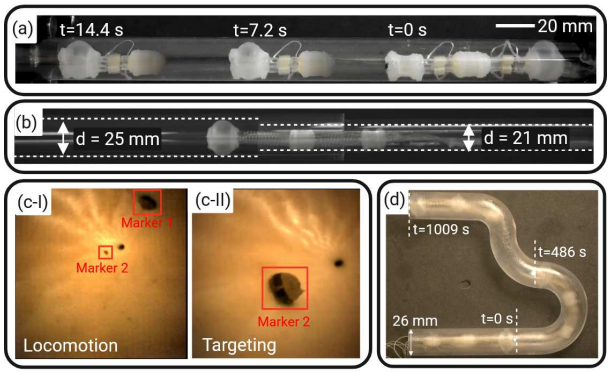

Fig. 5: Snapshots of Inchiscope during (a) locomotion baseline evaluation and (b) varied-diameter lumen test. (c-I, c-II) Locomotion and targeting markers in a lubricated compliant phantom. (d) Curvilinear navigation and observation test.

parameters $L = 13$, $\theta = \pi/2$, and the corresponding CC-model predicted trajectory. The overall RMSE across the five trajectories was 4.4±0.4 mm; the RMSE for x, y and z axes were 1.9±0.3, 2.1±0.2 mm and 3.3±0.5 respectively.

The dynamic response of the PBAs was evaluated by moving between the rest point to six evenly spaced points around a 38 mm radius circle representing 89 % of the Inchiscope's workspace. Figure 4(c-VII) shows the stepwise response of the system across the five repeats, with the tip position tracked in three spatial dimensions along with the graphed target position. The overall steady state RMSE of the tip was 3.2±3.6 mm. The rise time was 1.8±0.7 s and settling time 4.79±0.7 s. In the x and y axes, the actuator motion showed a small overshoot beyond the steady-state position, indicating inertial contributions and elastic recoil within the soft structure.

IV. Experimental Validation

A. Locomotion Baseline Evaluation

Locomotion was first evaluated in a rigid tube to provide a repeatable baseline which isolates the the locomotion mechanism from wall compliance, variable contact friction and lumen dimensional non-uniformities. A clear plastic tube diameter of 21 mm was selected to represent the lower bound of the small bowel (Figure 5(a)). Direct visualisation provides a clear overview of the attributes of the Inchiscope under locomotion, serving as the reference for cycle timing and step lengths in subsequent tests. The inchworm was operated in the full extension locomotion mode following the cycle pattern shown in Figure 3(b). To demonstrate the maximum movement speed, input pressures of positive 30 kPa and negative 60 kPa were cycled with each cycle step taking 500 ms, except for the PBA actuation steps (steps 2 and 5) which were 200 ms. The robot completed seven cycles with an average step length of 27.4±1.3 mm and covering 192 mm in 16.8 s, equating an average speed of ∼11.4 mm/s, as shown in the Supplementary Video (S1). A further rigid tube test, in which the lumen diameter increased from 21 mm to 25 mm , demonstrated the Inchiscope's ability to move through a varied diameter lumen (Figure 5(b)). Despite the stride length remaining similar (28.5±0.5 mm), implying no increased slipping, the speed

decreased to 7.1±0.1 mm/s as AB inflation cycle steps were increased to 900 ms, to account for the larger lumen.

B. Locomotion in Phantom Tissue

Locomotion was also assessed in a compliant 24 mm internal diameter small-bowel phantom (EasySurg Training System, HumanX Medical LLC, USA) to establish performance with compliant wall mechanics where axial stretch and local diameter changes can influence anchoring and traction. An endoscope was introduced from the distal end to provide internal visualisation while the Inchiscope advanced toward it; S1 shows synchronised views from the endoscope, the Inchiscope's onboard camera, and an external perspective. The AB cycle step lengths were increased to 600 ms to account for the larger diameter lumen and compliant walls, with bellows extension-contraction maintained at 200 ms, increasing the full cycle length to 2.8 s. The robot locomoted at a speed of 9.5±0.1 mm/s across three repeats of navigating the compliant lumen. A second set of tests were completed to evaluate the ability of the device within a lubricated (OptiLube, Optimum Medical) phantom, approximating the low-friction, mucus-lined environment of the small intestine. In this case, the Inchiscope locomoted at 8.6±0.2 mm/s across three tests: a 13.1 % decrease compared to the non-lubricated lumen.

C. Anchored Observation

Clinical tasks commonly require tip reorientation without axial advancement, and stable anchoring is essential to avoid unintended camera motion or tissue shear. To demonstrate the anchored observation control strategy, the central and proximal ABs were inflated to secure the Inchiscope within a small bowel simulator (Esophago-Gastro-Duodenoscopy (EGD) Simulator, Adam Rouilly), and the distal segment was actuated using the joystick interface to trace a circular trajectory. As shown in S1, the device remained stable and the tip orientation changed smoothly without abrupt motion, validating the CC-based joystick mapping for open-loop tip positioning. The anchored observation capability is further demonstrated inside of a compliant small bowel phantom, in which the Inchiscope seamlessly changes between the Full Extension and Anchored Observation modes to navigate through the phantom and point the camera towards a marker representing a target (Figure 5(c-I, c-II), Video S1).

D. Curvilinear Navigation and Observation

A curvilinear phantom was designed to emulate the more complex curvature and confined lumen encountered in the small bowel, as shown in Figure 5(d). This configuration incorporates sharp bends and reversals for evaluating locomotion and steering performance of the Inchiscope under more challenging conditions. A rigid tubular pathway measuring 410 mm in length with an internal diameter of 26 mm was fabricated. The path included a straight segment of 75 mm, followed by two alternating 90° bends with radii 30 mm and 45 mm respectively. A subsequent 180° bend on a 45 mm radius was incorporated to simulate a sharp reversal followed by a final 150 mm straight section.

To complete navigation through the phantom, the robot was operated in a tip-steering configuration, where the distal PBA segment pulled the body forward and steering was controlled via the joystick interface. Control was manually switched between extension-contraction and joystick steering to enable the user to reposition the robot during advancement through the different sections of the phantom. Full traversal required 17 minutes (see S1), reflecting the complexity of the narrow curvilinear path. The robot navigated through all curvature features without the need to reset anchors or reverse, demonstrating the effective tip positioning under joystick control.

V. Discussion and Conclusion

This work presents a miniaturised and modular soft robotic endoscope for navigation and observation of the small bowel. The design facilitates three unique control strategies which support the Inchiscope's versatility. Through characterisation of the individual soft components, maximum lumen dimensions and anchoring force of the robot were determined, as well as the extension, bending capabilities and accuracy of the PBAs. With the effectiveness of this tip control demonstrated by targeting markers within the lubricated phantom using a joystick. Accuracy of tip control could be improved with the integration of proprioceptive sensors for closed-loop control.

As summarised in Table I, the Inchiscope demonstrates substantially higher locomotion speeds (8.6 mm/s in a lubricated phantom) compared with prior soft inchworm devices, which typically remain below 3 mm/s. A key contributor is the double-PBA extensional architecture, enabling larger stride lengths than single-extension designs. Lubrication in the compliant phantom test reduced speed by 13 %, consistent with increased slipping under low-friction mucus-like conditions, yet the system still demonstrated reliable forward progress at speeds exceeding comparable devices. Although compliant wall and lubricated in-vitro tests cannot fully replicate dynamic in-vivo factors such as peristalsis and spatially varying tissue stiffness, the measured speeds provide a useful reference for small-bowel navigation performance. These results confirm that the inchworm-inspired locomotion method can deliver controlled advancement without external pushing forces, potentially reducing associated procedural risks associated with push-endoscopy [6].

In the curvilinear tube, locomotion slowed due to the requirement of manual control of the locomotion cycle to steer the device. The increased tether–wall interaction could also have contributed to a slower progression by reducing stride length through increased slipping. Despite this, the robot completed the route successfully, indicating that the anchoring and extension mechanisms remain effective even in tortuous geometries. Future improvements in automated steering, through computer vision based control, and tether management using low friction coatings and active feeding may further enhance performance in such environments.

From a translational perspective, the Inchiscope is well suited to a single-use strategy due to its low-cost elastomer construction, modular assembly, and reliance on pneumatic actuation, which requires only low pressures and minimal

air volumes, thereby reducing external hardware demands. While the current prototype uses exposed pneumatic lines and wiring, which may pose practical challenges for clinical deployment, future work will incorporate a protective outer sleeve to streamline the device profile and prevent entanglement. In addition, development of a balloon-tissue interaction model may support active anchoring control and tissue stress minimisation.

This approach addresses the limitations of existing inchworm endoscopes, which are too large for small bowel access, by combining miniaturisation (13 mm outer diameter) with self-propulsion and 3D tip control. The digital control architecture supports teleoperation and lays the foundation for future autonomous navigation and integration of therapeutic tools. Overall, the Inchiscope represents a novel three-balloon soft robotic approach towards safe and versatile small bowel exploration, bridging the gap between passive endoscopes and bulky inchworm systems designed for the colon.

REFERENCES

[1] H. F. Helander and L. Fändriks, "Surface area of the digestive tract – revisited," en, *Scandinavian Journal of Gastroenterology*, vol. 49, no. 6, pp. 681–689, Jun. 2014, ISSN: 0036-5521, 1502-7708.

[2] C. Hacking, S. Iqbal, and M. Saber, "3-6-9 rule (bowel)," en, in *Radiopaedia.org*, Feb. 2019.

[3] S. Alatab et al., "The global, regional, and national burden of inflammatory bowel disease in 195 countries and territories, 1990–2017: A systematic analysis for the global burden of disease study 2017," *The Lancet Gastroenterology Hepatology*, vol. 5, no. 1, pp. 17–30, 2020, ISSN: 2468-1253.

[4] J. Huang et al., "Incidence, risk factors, and temporal trends of small intestinal cancer: A global analysis of cancer registries," *Gastroenterology*, vol. 165, no. 3, pp. 600–612, 2023.

[5] G. V. Assche and P. Rutgeerts, "Medical management of postoperative recurrence in Crohn's disease," en, *Gastroenterology Clinics of North America*, vol. 33, no. 2, pp. 347–360, 2004.

[6] S. Ullah et al., "Complications of single-balloon enteroscopy," *World Journal of Gastroenterology*, vol. 31, no. 34, Sep. 2025.

[7] M. G. Shiha et al., "Device-assisted enteroscopy performance measures in the United Kingdom: DEEP-UK quality improvement project," *Endoscopy*, vol. 56, no. 03, pp. 174–181, 2024.

[8] M. Schneider, J. Höllerich, and T. Beyna, "Device-assisted enteroscopy: A review of available techniques and upcoming new technologies," *World Journal of Gastroenterology*, vol. 25, no. 27, pp. 3538–3545, 2019.

[9] A. J. Irvine, D. S. Sanders, A. Hopper, M. Kurien, and R. Sidhu, "How does tolerability of double balloon enteroscopy compare to other forms of endoscopy?" *Frontline Gastroenterology*, vol. 7, no. 1, pp. 41–46, 2016, ISSN: 2041-4137.

[10] S. S. Chauhan et al., "Enteroscopy," *Gastrointestinal Endoscopy*, vol. 82, no. 6, pp. 975–990, 2015.

[11] A. Mussetto et al., "Device-assisted enteroscopy: Are we ready to dismiss the spiral?" *World Journal of Gastroenterology*, vol. 30, no. 26, pp. 3185–3192, 2024.

[12] A. Giri, C. Girerd, J. Cervera-Torralba, M. T. Tolley, and T. K. Morimoto, "Inchigrab: An inchworm-inspired guided retraction and bending device for vine robots during colonoscopy," *IEEE/ASME Transactions on Mechatronics*, pp. 1–12, 2025.

[13] N. G. Kim et al., "External steering of vine robots via magnetic actuation," *Soft Robotics*, vol. 12, no. 2, pp. 159–170, 2025.

[14] J. Shi, K. Borvorntanajanya, K. Chen, E. Franco, and F. R. y. Baena, "Design, control, and evaluation of a novel soft everting robot for colonoscopy," *IEEE Transactions on Robotics*, vol. 41, pp. 4843–4859, 2025.

[15] S. Al Harthy et al., "Tip-growing robots: Design, theory, application," *IEEE Transactions on Robotics*, vol. 41, pp. 5511–5532, 2025.

[16] S. H. Kim and H. J. Chun, "Capsule Endoscopy: Pitfalls and Approaches to Overcome," *Diagnostics*, vol. 11, no. 10, p. 1765, 2021.

[17] X. Li, D. Zeng, H. Xu, Q. Zhang, and B. Liao, "Magnetic Actuation for Wireless Capsule Endoscopy in a Large Workspace Using a Mobile-Coil System," *Micromachines*, vol. 15, no. 11, p. 1373, 2024.

[18] W. A. Woods, S. J. Fusillo, and B. A. Trimmer, "Dynamic properties of a locomotory muscle of the tobacco hornworm *Manduca sexta* during strain cycling and simulated natural crawling," *Journal of Experimental Biology*, vol. 211, no. 6, pp. 873–882, Mar. 2008.

[19] X. Ren et al., "Robotic origami-based soft endoscope (rose) for minimally-invasive colonoscopy," *IEEE/ASME Transactions on Mechatronics*, pp. 1–12, 2025.

[20] L. Manfredi, E. Capoccia, G. Ciuti, and A. Cuschieri, "A Soft Pneumatic Inchworm Double balloon (SPID) for colonoscopy," *Scientific Reports*, vol. 9, no. 1, p. 11 109, 2019.

[21] A. Trecca, F. Catalano, A. Bella, and R. Borghini, "Robotic colonoscopy: Efficacy, tolerability and safety. Preliminary clinical results from a pilot study," en, *Surgical Endoscopy*, vol. 34, no. 3, pp. 1442–1450, Mar. 2020.

[22] Y. Yao, L. He, and P. Maiolino, "A simulation-based toolbox to expedite the digital design of bellow soft pneumatic actuators," in *2022 IEEE 5th International Conference on Soft Robotics (RoboSoft)*, 2022, pp. 29–34.

[23] D. O'Brien and D. Lane, "3d force control system design for a hydraulic parallel bellows continuum actuator," in *2001 IEEE International Conference on Robotics and Automation (ICRA)*, vol. 3, 2001, 2375–2380 vol.3.

[24] R. J. Webster and B. A. Jones, "Design and Kinematic Modeling of Constant Curvature Continuum Robots: A Review," *The International Journal of Robotics Research*, vol. 29, no. 13, pp. 1661–1683, 2010.